Progress In Electromagnetics Research M, Vol. 105, 45–54, 2021

High-Sensitive Mid-Infrared Photonic Crystal Sensor Using Slotted-Waveguide Coupled-Cavity

Hadjira Tayoub[1, 2, *], Abdesselam Hocini[1], and Ahlam Harhouz[1]

Abstract—In this paper, a novel high-sensitive mid-infrared photonic crystal-based slotted-waveguide coupled-cavity sensor to behave as a refractive index sensing device is proposed at a mid-infrared wavelength of 3.9 µm. We determine the sensitivity of our sensor by detecting the shift in the resonance wavelength as a function of the refractive index variations in the region around the cavity. Comparison shows that mid-infrared photonic crystal-based slotted-waveguide coupled-cavity has higher sensitivity to refractive index changes than mid-infrared photonic crystal-based slotted-waveguide. The sensitivity can be improved from 938 nm/per refractive index unit (RIU) to 1161 nm/RIU within the range of $n = 1$–1.05 with an increment of 0.01 RIU in the wavelength range of 3.3651 µm to 4.1198 µm by creating a microcavity within the proposed structure, calculated quality factor (Q-factor) of 1.0821×10^7 giving a sensor figure of merit (FOM) up to 2.917×10^6, and a low detection limit of 3.9×10^{-6} RIU. Furthermore, an overall sensitivity is calculated to be around $S = 1343.2$ nm/RIU for the case of higher refractive indices of analytes within the range of $n = 1$–1.2 with an increment of 0.05 RIU. The described work and the achieved results by performing 2D-finite-difference time-domain (2D-FDTD) simulations confirm the ability to realize a commercially viable miniaturized and highly sensitive mid-infrared photonic crystal-based slotted-waveguide coupled-cavity sensor.

1. INTRODUCTION

Photonic crystals (PhCs), which can be considered as one of the most progressive recent photonic technologies [1–4] were first proposed by Yablonvitch [5] and John [6]. Their theoretical inception photonic crystals (PCs) have attracted important attention in the scientific community due to their unique ability to guide and trap light in length scales of the wavelength of light [7]. Optical sensors show immunity to electromagnetic interference, rapid response time, room temperature operation, and offline monitoring where the signal can be monitored far from the sensing location [8, 9]. Conventional optical sensors own high selectivity, stability, and real-time detection capability. However, the photonic crystal (PhC) based sensing technique takes a lead because of its compact structure and the possibility to control and manipulate the properties of light [10–12].

An innovative player in the area of optical sensors is slotted photonic crystal [13–24]. Slotted photonic crystals are usually fabricated in silicon-on-insulator substrates to squeeze light down into very small volumes of air. This strong confinement and control of the propagation of light in the air of the slot is the basic benefit of the slotted photonic crystal, as it improves strong light-matter interactions [25] and achieves high detection sensitivity. Slotted-waveguides were first presented in 2004 by Almeida et al. [26]. They have seen much attention in various applications due to their unusual optical properties. They permit strong spatial confinement of light within a narrow air-slot inside a material of high refractive index by confining light in what is known as a "slotted-waveguide," whereby the discontinuity of the optical field at a dielectric interface is exploited to shift every guided mode of

Received 12 July 2021, Accepted 19 September 2021, Scheduled 1 October 2021

* Corresponding author: Hadjira Tayoub (hadjira.tayoub@univ-msila.dz).

[1] Laboratoire d'Analyse des Signaux et Systèmes, Department of Electronics, University of M'Sila BP. 166, Route Ichebilia, M'Sila 28000, Algeria. [2] Research Center in Industrial Technologies CRTI, P. O. Box 64, Cheraga, Algiers 16014, Algeria.

the photonic crystal waveguide towards higher frequencies and to pull the fundamental mode into the gap [27].

Recently, integrated mid-infrared (mid-IR) photonics have gained considerable attention because silicon is optically transparent from 1.1 µm to 8 µm [28], and most of the gases have their characteristic absorption peak in the mid-IR range [29], and as a result, Mid-IR photonic crystal can serve as an ideal, with enormous potential for new applications in optical interconnects and sensing [28, 30–32].

In many previous works, the slotted photonic crystal in the near-IR telecom wavelengths around 1550 nm has been studied. Barrios et al. [33] have proposed an integrated biochemical sensor based on a slot-waveguide microring resonator, and a linear shift of the resonant wavelength with an increasing ambient refractive index of 212 nm/RIU has been observed. Di Falco et al. [14] have suggested slotted photonic crystal waveguides and cavities supporting resonant modes in air, and the sensitivity of 585 nm/RIU has been attained. On the other hand, limited works have been dedicated to studying slotted photonic crystals in the mid-IR. Among modern works, Mid-IR slotted photonic crystal waveguides in silicon-on-sapphire working in the mid-IR regime have been well demonstrated by Zou et al. [7, 34–36]. A T-slotted photonic crystal sensor was designed and proposed by Turduev et al. [37], and the sensitivity of 500 nm/RIU has been achieved. A mid-IR refractive index sensor based on 2D photonic crystal coupled cavity-two waveguides was also investigated in [38], and the sensitivity of 758 nm/RIU for a refractive index range of $n = 1.01$–1.04 and sensitivity of 500 nm/RIU for a refractive index range of $n = 1.33$–1.331 have been attained. In this work, we propose a novel high-sensitive mid-IR photonic crystal sensor with beyond 1000 nm/RIU sensitivity and Q-factor of more than 10^7.

In this context, to contribute to the works already done in the burgeoning range of mid-IR (at 3.9 µm), a novel mid-IR photonic crystal-based slotted-waveguide coupled-cavity refractive index sensing in mid-IR range design has been proposed. As our idea promises to improve the sensitivity, high sensitivity of $S = 1343.2$ nm per refractive index unit (RIU) has been achieved within the range of $n = 1$–1.2 with an increment of 0.05 RIU. The behavior of the designed sensor is analyzed using the 2D-finite-difference time-domain (2D-FDTD) method from the RSoft software package.

2. DESIGN OF THE SLOTTED-WAVEGUIDE COUPLED-CAVITY STRUCTURE

In order to explore the photonic crystal-based slotted-waveguide coupled-cavity for mid-IR optical refractive index sensing, we propose a structure that consists of a hexagonal lattice with a size of photonic crystal of (49×29), arranged periodically with a lattice constant (a) equal to 1.1 µm, and the effective index profile of the silicon slab has been calculated to be 2.654 by the effective index method [39], while the ratio of the radii of air holes (r) and lattice constant is 0.29.

3. NUMERICAL RESULTS AND DISCUSSION

The designed photonic crystal structure having a photonic bandgap in the wavelength range of 3.3651 µm to 4.1198 µm for TM-polarized wave is shown in Figure 1, which is calculated by 2D Plane Wave Expansion (2D-PWE) method. In Figure 1, the used symbols Γ, M, K signify the edges of Brillouin zone. The photonic band structure principally depends on the radius of holes and the lattice constant of the structure.

The photonic crystal-based slotted-waveguide is realized by removing a single row of air holes along the ΓK direction, thus creating a $W1$ waveguide and replacing it with a narrow air slot due to which the interaction of optical mode with the analyte increases because of the reduced group velocity and thereby achieves further improvement in the sensitivity [25]. The width and length of the air slot are $0.27a$ and $44a$, respectively (Figure 2).

Since full three-dimensional calculations require a great amount of memory space and consume a very long time, 3D simulations are reduced to simpler approximated two-dimensional simulations. In this paper, 2D simulation has been done using the effective index of the structure to preserve enough accuracy [40]. 2D FDTD simulation with a grid size of 0.05 of the proposed structure's result is shown in Figure 3. Figure 3(a) illustrates the evolution of the normalized transmission spectrum as a function of wavelengths for different refractive indices ranging from $n = 1$ to $n = 1.05$, and the increase of the refractive index shifts the transmission spectrum to longer wavelengths. The evolution of the cut-off

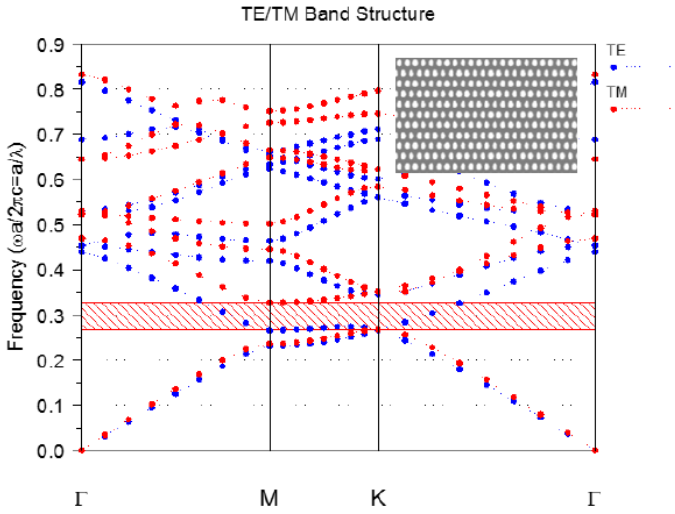

Figure 1. Band structure diagram of the connected photonic crystal structure.

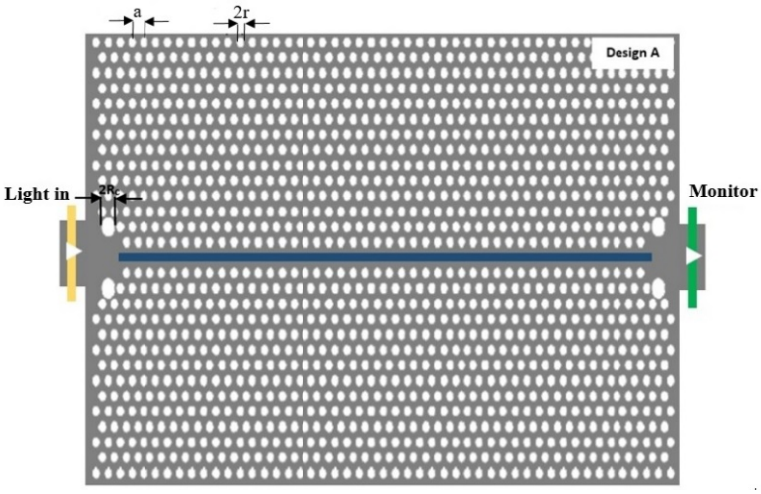

Figure 2. Schematic of the photonic crystal-based slotted-waveguide sensor, for which the optimized $R_C = 0.56a$.

wavelength shift as a function of the refractive index is shown in Figure 3(b). We can clearly notice that the shift is linear and equal to 51.9 nm for a refractive index of $n = 1.05$. A shift in the resonance wavelength of 9.38 nm for $\Delta n = 0.01$ and consequently, sensitivity of 938 (nm/RIU) is observed, and the high sensitivity can be explained by the strong optical field confinement and the correspondingly improved light intensity on the slotted-waveguide.

It is verified that the proposed structure has the potentiality to maintain a sensitivity over a wide refractive index ranging from $n = 1$ to $n = 1.2$. The results show that the sensitivity of the proposed structure could be up to 899 nm/RIU. Figure 4(a) given below shows the evolution of the normalized transmission spectrum as a function of the wavelengths for different refractive indices, and the curves show that with the increase of the refractive index, the position of the transmission spectrum shifts to higher wavelengths. It can be noticed from Figure 4(b) that as the refractive index increases, there is a corresponding shift in the cut-off wavelength and consequently, and the sensitivity of 899 (nm/RIU) is observed.

The photonic crystal-based slotted-waveguide coupled-cavity sensor is more sensitive near the region of the narrow air slot, where the electromagnetic field is the most intense, and the region near the slot

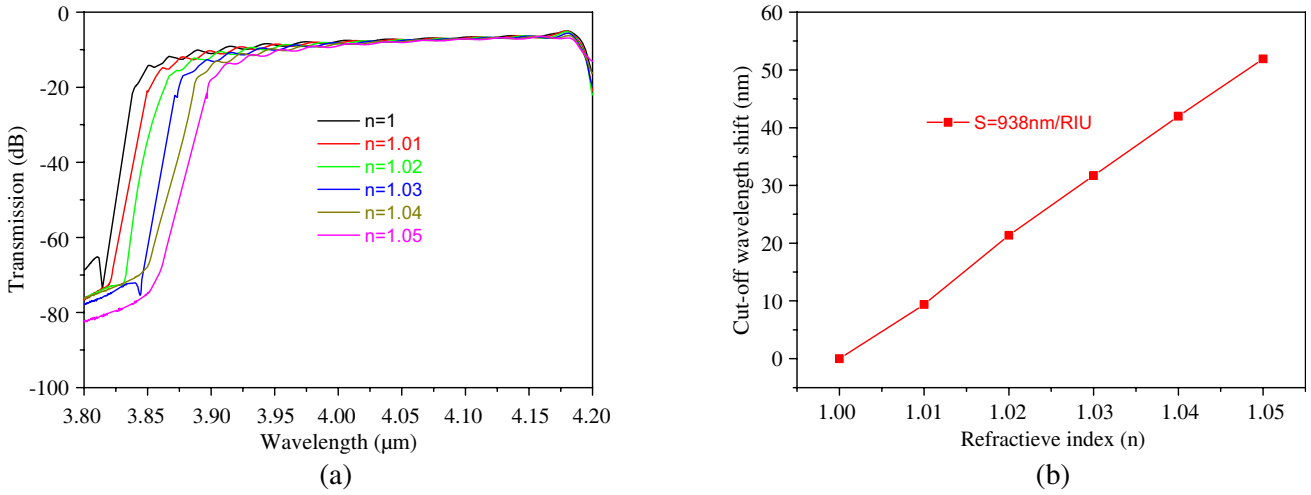

Figure 3. (a) Normalized transmission spectrum of the proposed design as a function of wavelength for different refractive indices ranging from $n = 1$ to $n = 1.05$ with an increment of $\Delta n = 0.01$, (b) shifts in the cut-off wavelength of the proposed structure with changes of the refractive index values, bring on sensitivity of 938 nm/RIU.

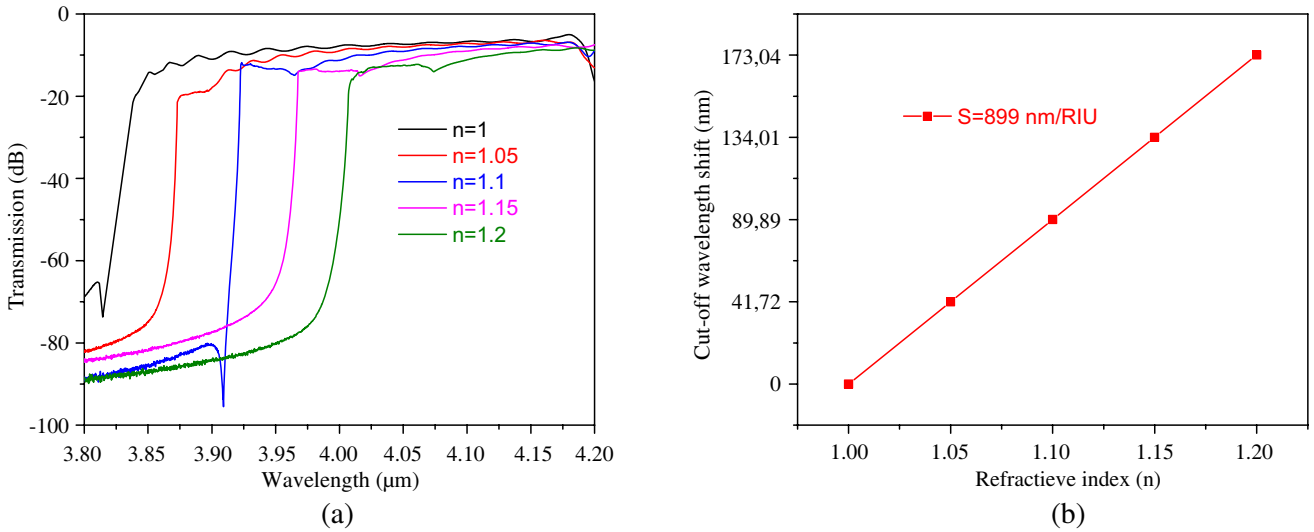

Figure 4. (a) Normalized transmission spectrum of the proposed design as a function of the wavelength for different refractive indices ranging from $n = 1$ to $n = 1.2$ with an increment of $\Delta n = 0.05$, (b) shifts in the cut-off wavelength of the proposed structure with changes of refractive index values, bring on sensitivity of 899 nm/RIU.

has been modified in order to obtain higher sensitivity [41]. Several approaches are used to create a cavity resonance such as increasing or reducing the radius of particular holes [42]. In the modified design (Figure 5), a microcavity was created within the structure by increasing the radius of the black-colored defected holes to confine light within the cavity, and by shifting (in the x-direction) in the opposite direction the microcavity. Such displacement allows achieving a smoother transition between the slotted waveguide and the defected holes, hence, resulting in a high-quality factor. The air hole shift S_x is scanned from a shift of $0.05a$ to a maximum shift of $0.15a$ with a step of 0.05 in order to enhance the sensitivity of the device.

Normalized transmission spectrum with and without a microcavity as a function of the wavelength is presented in Figure 6(a). As previously mentioned, creating a microcavity in the vicinity of the air

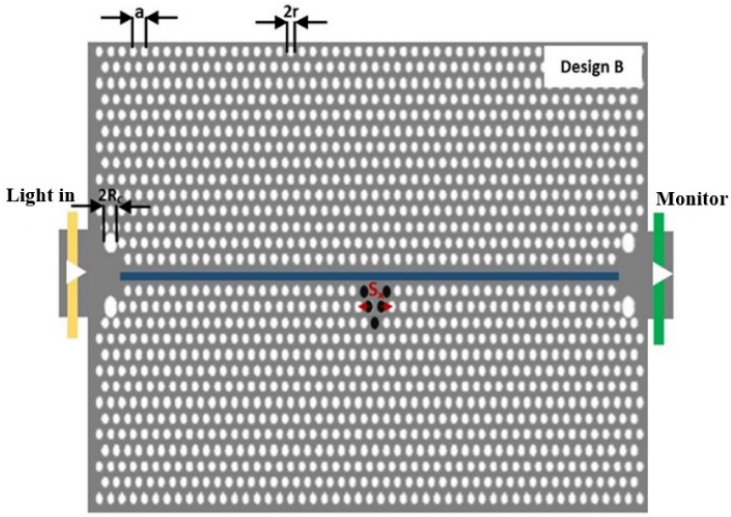

Figure 5. The modified photonic crystal-based slotted-waveguide coupled-cavity sensor where the holes (showing in black color) forming a resonant cavity to accomplish higher sensitivity.

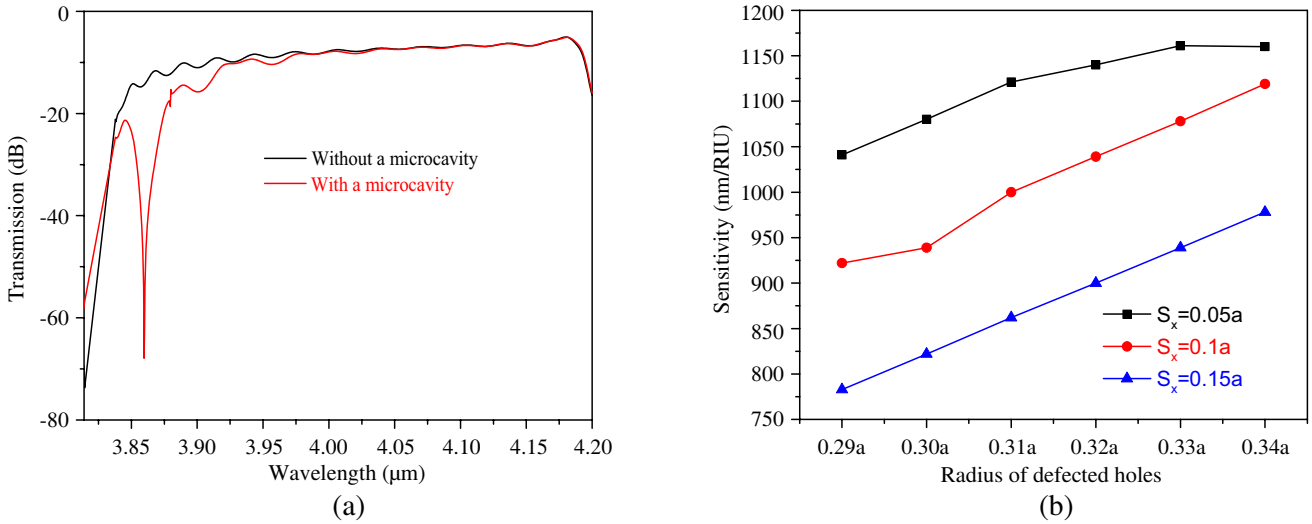

Figure 6. (a) Normalized transmission spectrum with and without a microcavity as a function of the wavelength, (b) relationships of the sensitivity of the improved device to the defected holes radius for different values of the lattice shift S_x.

slot improves the light-matter interaction level.

Figure 6(b) shows the sensitivity of the improved device versus different values of the defected holes radius ranging from $0.29a$ to $0.34a$ with a step of 0.01. For different values of the lattice shift S_x, the resonant frequency between the resonant cavity and the air slot will shift. A shift in the resonance wavelength of 11.61 nm for $\Delta n = 0.01$ is attained, and a comparatively much higher sensitivity of 1161 (nm/RIU) is achieved. As expected, by increasing the defected holes radius, an improvement in the sensitivity of the device is observed. As the radius of defected holes is increased, shifting the two centered holes in the microcavity slightly in the opposite direction altogether provides an improved coupling between the slotted waveguide and the defected holes leading to enhancing the device performance.

Q-factor measures the selectivity level of the sensor, and the desired resonant peak should be as sharp as possible to enhance the Q-factor [43]. In this paper, the simulation of the Q-factor is carried out

by 2D FDTD method combined with fast harmonic analysis using the Q-finder model in RSoft software. The calculated Q-factor of the resonant mode is as high as 1.0821×10^7 which is sufficiently high for sensing applications. The figure of merit (FOM) of the device for sensing is extremely high (2.917×10^6) because of the high sensitivity and Q-factor of the sensor. A summary of all the aforementioned results is presented in Table 1.

Table 1. List of sensitivity, Q-factor, and FOM values for the improved device.

Radius of the defected holes	Lattice shift S_x	Sensitivity (nm/RIU)	Q-factor	FOM
$0.29a$	$0.05a$	1041	1.821×10^7	2.917×10^6
	$0.1a$	922	41604	9886.31
	$0.15a$	783	12035	2412.28
$0.30a$	$0.05a$	1080	2.4734×10^5	6.9266×10^4
	$0.1a$	939	2.47×10^5	4.9646×10^4
	$0.15a$	822	44268	9338.4
$0.31a$	$0.05a$	1121	1.1192×10^5	3.25×10^4
	$0.1a$	1000	1.87×10^6	5.58×10^5
	$0.15a$	862	48296	10710.63
$0.32a$	$0.05a$	1140	44354	13132.23
	$0.1a$	1039	50053	13481.37
	$0.15a$	900	28173	6538.95
$0.33a$	$0.05a$	1161	64121	19339.84
	$0.1a$	1078	8.03×10^5	2.2467×10^4
	$0.15a$	939	26870	6521.18
$0.34a$	$0.05a$	1160	2.2841×10^5	6.8843×10^4
	$0.1a$	1119	1.1583×10^6	3.3662×10^5
	$0.15a$	978	36822	9325.64

Extensive simulation results demonstrate that the modified photonic crystal-based slotted-waveguide coupled-cavity sensor can possess high sensitivity, and a high Q-factor ($S = 1343.2$ nm/RIU (Figure 7) and a high Q-factor of 15913 are the best-optimized case for $n = 1.1$) for the optimized parameters, with radius of the defected holes equal to $0.34a$ and a lattice shift S_x of $0.05a$. These results confirm the viability of the modified sensor in the mid-infrared for the case of higher refractive indices of analytes within the range of $n = 1$–1.2 with an increment of 0.05 RIU.

To study the performance of the proposed sensor, methane (CH_4) gas sensing was considered. CH_4 sensing is essential in both environmental and industrial scopes [44]. It is chosen as the target gas, since it is the main component of natural gas and has absorption features in several regions of the infrared spectral range (0.75–14 µm) [45].

The refractive index of each gas was selected for the mid-Infrared wavelength. Figure 8 illustrates the transmission spectrum of the slotted photonic crystal waveguide immersed in air ($n = 1.000265$), and methane gas CH_4 ($n = 1.0004365$) for a radius of defected holes equal to $0.34a$ and a lattice shift S_x equal to $0.15a$. The shift in the wavelength corresponds to the high sensitivity of 1224.48 (nm/RIU), high Q-factor of 1.0397×10^5, and low detection limit of 2.25×10^{-4} RIU. The achieved results confirm that the proposed mid-infrared photonic crystal-based slotted-waveguide coupled-cavity sensor is well-suited to act as a mid-infrared gas sensor.

A brief comparison between our results and some of the results already published in scientific research papers in the last five years is represented in Table 2. The proposed sensor showed remarkable higher sensitivity, high Q-factor, low detection limit, and high figure of merit (FOM) due to the increase in light-matter interaction.

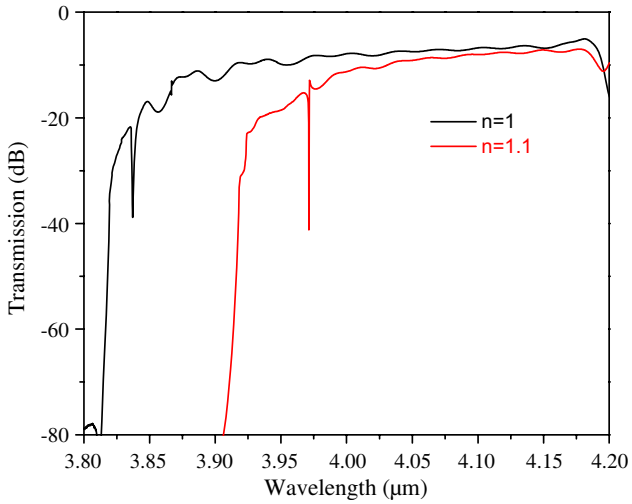

Figure 7. Normalized transmission spectrum of the proposed design as a function of the wavelength for $n = 1$ and $n = 1.1$.

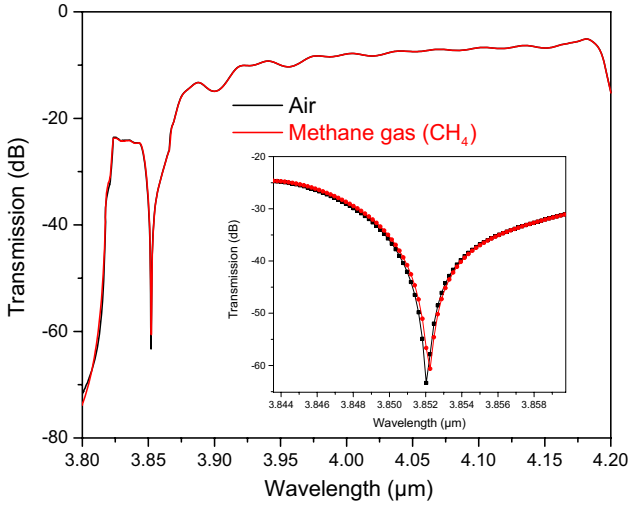

Figure 8. Transmission spectrum of the photonic crystal-based slotted-waveguide coupled-cavity sensor immersed in air ($n = 1.000265$), and methane gas ($n = 1.0004365$).

Table 2. Comparison between the literatures and the proposed sensor.

Sensing structure	Sensitivity (nm/RIU)	Detection limit (RIU)	Year
[30] Mid-IR gas sensor based on point-defect PhC nanocavities H1 PhC cavity L3 PhC cavity	 234 268	 8.84×10^{-4} 1.50×10^{-4}	2020
[46] Mid-IR RI sensor formed by slotted PhCW	1150	—	2017
[37] Mid-IR T-shaped PhC for optical RI sensing	1040	—	2017
Mid-IR PhC sensor using slotted-waveguide coupled-cavity	1343.2	3.9×10^{-6}	—

4. CONCLUSION

As we draw a conclusion to this article, the design and simulation of a mid-infrared photonic crystal-based slotted-waveguide coupled-cavity for refractive index sensing has been profitably presented. The best-calculated sensitivity of the proposed slotted photonic crystal sensor operating at mid-IR (around $\lambda = 3.9\,\mu m$) is equal to 938 nm/RIU within the range of $n = 1$–1.05 with an increment of 0.01 RIU, and equivalent to 899 nm/RIU within the range of $n = 1$–1.2 with an increment of 0.05 RIU. Additionally, an improved sensitivity equal to 1161 nm/RIU within the range of $n = 1$–1.05 with an increment of 0.01 RIU, and as good as 1343.2 nm/RIU within the range of $n = 1$–1.2 with an increment of 0.05 RIU can be obtained by creating a microcavity in the area near the air slot by changing the radius and the position of specific holes in the structure. Additionally, using the proposed sensor for methane gas sensing in the mid-infrared application reveals high sensitivity of 1224.48 (nm/RIU). The reported results show the improvement in the limit of detection with high sensitivity, high Q-factor, high transmittance, and small size. Consequently, our enhanced sensor is well-matched for applications in mid-IR sensing, and it would be a great potential platform for realizing mid-IR lab-on-chip photonic circuits.

REFERENCES

1. Ge, X., Y. Shi, and S. He, "Ultra-compact channel drop filter based on photonic crystal nanobeam cavities utilizing a resonant tunneling effect," *Opt. Lett.*, Vol. 39, 6973, 2014.
2. Lin, C., H. Subbaraman, A. Hosseini, A. X. Wang, L. Zhu, R. T. Chen, C. Lin, H. Subbaraman, A. Hosseini, A. X. Wang, L. Zhu, and R. T. Chen, "Silicon nanomembrane based photonic crystal waveguide array for wavelength-tunable true-time-delay lines," *Appl. Phys. Lett.*, Vol. 051101, 1, 2012.
3. Gao, Y., R. Shiue, X. Gan, L. Li, C. Peng, I. Meric, L. Wang, A. Szep, D. Walker, J. Hone, and D. Englund, "High-speed electro-optic modulator integrated with graphene-boron nitride heterostructure and photonic crystal nanocavity," *Nano Lett.*, 2015.
4. Harhouz, A., A. Hocini, and H. Tayoub, "Ultracompact gas-sensor based on a 2D photonic crystal waveguide incorporating with tapered microcavity," *IOP Conf. Ser. Mater. Sci. Eng.*, Vol. 1046, 012001, 2021.
5. Yablonovitch, E., "Inhibited spontaneous emission in solid-state physics and electronics," *Phys. Rev. Lett.*, Vol. 58, 2059, 1987.
6. John, S., "Strong localization of photons in certain disordered dielectric superlattices," *Phys. Rev. Lett.*, Vol. 58, 2486, 1987.
7. Zou, Y., S. Chakravarty, R. T. Chen, Y. Zou, S. Chakravarty, and R. T. Chen, "Mid-infrared silicon-on-sapphire waveguide coupled photonic crystal microcavities," *Appl. Phys. Lett.*, Vol. 081109, 2015.
8. Hodgkinson, J. and R. P. Tatam, "Optical gas sensing: A review," *Meas. Sci. Technol.*, Vol. 24, 2013.
9. Seitz, W. R., "Chemical sensors based on fiber optics," *Anal. Chem.*, Vol. 56, 1984.
10. Shruti, R. K. Sinha, and R. Bhattacharyya, "Photonic crystal slab waveguide-based infiltrated liquid sensors: Design and analysis," *J. Nanophotonics*, Vol. 5, 053505, 2011.
11. Goyal, A. K. and S. Pal, "Design and simulation of high-sensitive gas sensor using a ring-shaped photonic crystal waveguide," *Phys. Scr.*, Vol. 90, 25503, 2015.
12. Tung, B. T., H. M. Nguyen, D. V. Dao, S. Rogge, H. W. M. Salemink, and S. Sugiyama, "Strain sensitive effect in a triangular lattice photonic crystal hole-modified nanocavity," *IEEE Sens. J.*, Vol. 11, 2657, 2011.
13. Di Falco, A., L. O. Faolain, T. F. Krauss, A. Di Falco, L. O. Faolain, and T. F. Krauss, "Dispersion control and slow light in slotted photonic crystal waveguides," *Appl. Phys. Lett.*, Vol. 083501, 2006, 2014.
14. Di Falco, A., L. O. Faolain, T. F. Krauss, A. Di Falco, L. O. Faolain, and T. F. Krauss, "Chemical sensing in slotted photonic crystal heterostructure cavities," *Appl. Phys. Lett.*, Vol. 063503, 6, 2011.
15. Scullion, M. G., A. Di Falco, and T. F. Krauss, "Biosensors and bioelectronics slotted photonic crystal cavities with integrated microfluidics for biosensing applications," *Biosens. Bioelectron.*, Vol. 27, 101, 2011.
16. Lai, W., S. Chakravarty, X. Wang, C. Lin, and R. T. Chen, "On-chip methane sensing by near-IR absorption signatures in a photonic crystal slot waveguide," *Opt. Lett.*, Vol. 36, 984, 2011.
17. Lai, W., S. Chakravarty, X. Wang, C. Lin, R. T. Chen, W. Lai, S. Chakravarty, X. Wang, and C. Lin, "Photonic crystal slot waveguide absorption spectrometer for on-chip near-infrared spectroscopy of xylene in water," *Appl. Phys. Lett.*, Vol. 023304, 2009, 2014.
18. Jágerská, J., H. Zhang, Z. Diao, N. Le Thomas, and R. Houdré, "Refractive index sensing with an air-slot photonic crystal nanocavity," *Opt. Lett.*, Vol. 35, 2523, 2010.
19. Wang, B., M. A. Dündar, R. Nötzel, F. Karouta, R. W. van Der Heiiden, and S. He, "Photonic crystal slot nanobeam slow light waveguides for refractive index sensing," *IEEE Trans. Inf. Theory*, Vol. 39, 966, 1993.
20. Kwon, S.-H., T. Sünner, M. Kamp, and A. Forchel, "Optimization of photonic crystal cavity for chemical sensing," *Opt. Express*, Vol. 16, 11709, 2008.

21. Lin, S., J. Hu, L. Kimerling, and K. Crozier, "Design of nanoslotted photonic crystal waveguide cavities for single nanoparticle trapping and detection," *Opt. Lett.*, Vol. 34, 3451, 2009.
22. Kurt, H., M. N. Erim, and N. Erim, "Chemical various photonic crystal bio-sensor configurations based on optical surface modes," *Sensors Actuators B. Chem.*, Vol. 165, 68, 2012.
23. Kassa-Baghdouche, L. and E. Cassan, "Sensitivity analysis of ring-shaped slotted photonic crystal waveguides for mid-infrared refractive index sensing," *Opt. Quantum Electron.*, Vol. 51, 2019.
24. Elshahat, S., I. Abood, Z. Liang, J. Pei, and Z. Ouyang, "Elongated-hexagonal photonic crystal for buffering, sensing, and modulation," *Nanomaterials*, Vol. 11, 1, 2021.
25. Scullion, M. G., T. F. Krauss, and A. Di Falco, "Slotted photonic crystal sensors," *Sensors (Switzerland)*, Vol. 13, 3675, 2013.
26. Almeida, V. R., Q. Xu, C. A. Barrios, and M. Lipson, "Guiding and confining light in void nanostructure," *Opt. Lett.*, Vol. 29, 1209, 2004.
27. Di Falco, A., L. O. Faolain, and T. F. Krauss, "Photonic crystal slotted slab waveguides," *Photonics Nanostructures — Fundam. Appl.*, 38, 2008.
28. Soref, R., "Mid-infrared photonics in silicon and germanium," *Nat. Photonics*, Vol. 4, 495, 2010.
29. Goyal, A. K., H. S. Dutta, and S. Pal, "Recent advances and progress in photonic crystal-based gas sensors," *J. Phys. D. Appl. Phys.*, Vol. 50, 2017.
30. Kassa-Baghdouche, L. and E. Cassan, "Mid-infrared gas sensor based on high-Q/V point-defect photonic crystal nanocavities," *Opt. Quantum Electron.*, 2020.
31. Zouache, T. and A. Hocini, "Mid-infrared micro-displacement measurement with a bidimensional silicon photonic crystal," *Progress In Electromagnetics Research Letters*, Vol. 91, 77–83, 2020.
32. Rostamian, A., E. Madadi-Kandjani, H. Dalir, V. J. Sorger, and R. T. Chen, "Towards lab-on-chip ultrasensitive ethanol detection using photonic crystal waveguide operating in the mid-infrared," *Nanophotonics*, Vol. 10, 1675, 2021.
33. Barrios, C. A., K. B. Gylfason, B. Sánchez, A. Griol, H. Sohlström, M. Holgado, and R. Casquel, "Slot-waveguide biochemical sensor," *Opt. Lett.*, Vol. 32, 3080, 2007.
34. Zou, Y., S. Chakravarty, P. Wray, and R. T. Chen, "Mid-infrared holey and slotted photonic crystal waveguides in silicon-on-sapphire for chemical warfare simulant detection," *Sensors Actuators, B Chem.*, Vol. 221, 1094, 2015.
35. Zou, Y., H. Subbaraman, S. Chakravarty, X. Xu, A. Hosseini, W.-C. Lai, and R. T. Chen, "Integrated strip and slot waveguides in silicon-on-sapphire for mid infrared VOC detection in water," *Conference on Silicon Photonics IX*, Vol. 8990, 89900X, 2014.
36. Zou, Y., H. Subbaraman, S. Chakravarty, X. Xu, A. Hosseini, W.-C. Lai, and R. T. Chen, "Grating-coupled silicon-on-sapphire integrated slot waveguides operating at mid-infrared wavelengths," *Opt. Lett.*, Vol. 39, 3070, 2014.
37. Turduev, M., I. H. Giden, C. Babayi, H. Kurt, and K. Staliunas, "Chemical mid-infrared T-shaped photonic crystal waveguide for optical refractive index sensing," *Sensors Actuators B Chem.*, Vol. 245, 765, 2017.
38. Tayoub, H., A. Hocini, and A. Harhouz, "Mid-infrared refractive index sensor based on a 2D photonic crystal coupled cavity-two waveguides," *Instrum. Mes. Métrologie*, Vol. 18, 165, 2019.
39. Qiu, M., "Effective index method for heterostructure-slab-waveguide-based two-dimensional photonic crystals," *Appl. Phys. Lett.*, Vol. 1163, 10, 2002.
40. Vakili, M. and M. Noori, "Highly efficient elliptical microcavity refractive index sensor with single detection unit," *Opt. Quantum Electron.*, Vol. 51, 1, 2019.
41. Dutta, H. S. and S. Pal, "Design of a highly sensitive photonic crystal waveguide platform for refractive index based biosensing," *Opt. Quantum Electron.*, Vol. 45, 907, 2013.
42. Pal, S., E. Guillermain, R. Sriram, B. Miller, and P. M. Fauchet, "Microcavities in photonic crystal waveguides for biosensor applications," *Proc. SPIE*, Vol. 7553, 755304, 2010.
43. Mohammed, N. A., M. M. Hamed, A. A. M. Khalaf, A. Alsayyari, and S. El-Rabaie, "High-sensitivity ultra-quality factor and remarkable compact blood components biomedical sensor based on nanocavity coupled photonic crystal," *Results Phys.*, Vol. 14, 102478, 2019.

44. Gas-cell, C. P., W. Ye, Z. Tu, X. Xiao, A. Simeone, J. Yan, T. Wu, F. Wu, C. Zheng, and F. K. Tittel, "A NDIR mid-infrared methane sensor with a compact pentahedron gas-cell," *Sensors*, Vol. 20, 2020.
45. Del, R., P. Moreira, C. Roberto, and D. S. Filho, "Detection of methane plumes using airborne midwave infrared (3–5 μm) hyperspectral data," *Remote Sens.*, Vol. 2, 1, 2018.
46. Kassa-baghdouche, L. and E. Cassan, "Mid-infrared refractive index sensing using optimized slotted photonic crystal waveguides," *Photonics Nanostructures — Fundam. Appl.*, Vol. 28, 32, 2017.